Eur. Phys. J. A **30**, 47–64 (2006)
DOI 10.1140/epja/i2006-10107-8

THE EUROPEAN PHYSICAL JOURNAL A

High-energy probes

A. Bonasera[a], R. Coniglione, and P. Sapienza

INFN - Laboratori Nazionali del Sud, Via S. Sofia 62, I-95123 Catania, Italy

Received: 13 February 2006 /
Published online: 12 October 2006 –

Abstract. We review some results on energetic particle production in heavy-ion collisions below roughly 100 A·MeV, both theoretically and experimentally. We discuss the possible mechanisms of particle production, as well as the possibility to gather information on the nuclear equation of state (EOS) from data. Results on subthreshold pions, energetic photons, nucleons and light charged particles ($Z \leq 2$) are discussed and contrasted to microscopic models. Important information about the first stages of the reaction are obtained by such probes. At present, we can conclude that we have at least a qualitative understanding of the processes involved when such particles are produced. However, a quantitative determination of relevant EOS parameters is still missing. The production mechanism close to the kinematical threshold (incoherent, cooperative or statistical) is not completely elucidated either. This calls for new data using more modern detector systems and comparison to more refined microscopic models.

PACS. 25.70.-z Low and intermediate energy heavy-ion reactions – 25.75.Dw Particle and resonance production

1 Introduction

One among the many purposes to collide heavy ions at beam energies below 100 A·MeV is the study of the nuclear-matter equation of state (EOS) at finite densities and temperatures. In fact, in such reactions the colliding nuclei are compressed and heated up. After some tens of fm/c, a maximum compression is reached and a compound system is formed, which then expands and, depending on the excitation energy reached, might break into many pieces (multi-fragmentation). In such a scenario there are many factors at play. In the compression stage the dynamics is ruled by the EOS of the system and by the viscosity. Thus data sensitive to the early stage such as energetic protons, neutrons and more complex fragments, as well as photons and pions, will give valuable information and put constraints on these fundamental ingredients of the nuclear interaction.

In the intermediate-energy regime, different powerful detection systems available (MEDEA [1], INDRA [2], NIMROD [3], CHIMERA [4], TAPS [5]), MINIBALL [6], MULTICS [7] (see the contribution by de Souza *et al.* in this topical issue) allow to study with great accuracy energetic and subthreshold particle emission. The comparison of experimental data (impact parameter dependence of particle multiplicity, removed excitation energy, angular distributions, slopes of energy spectra, ...) with the prediction of transport models can put constraints on basic properties of hadronic matter as the in medium Nucleon-Nucleon (NN) cross-section, nuclear-matter compressibility, mean-field properties, or the relevance of two-body *versus* three-body forces. It has been shown, for exam-

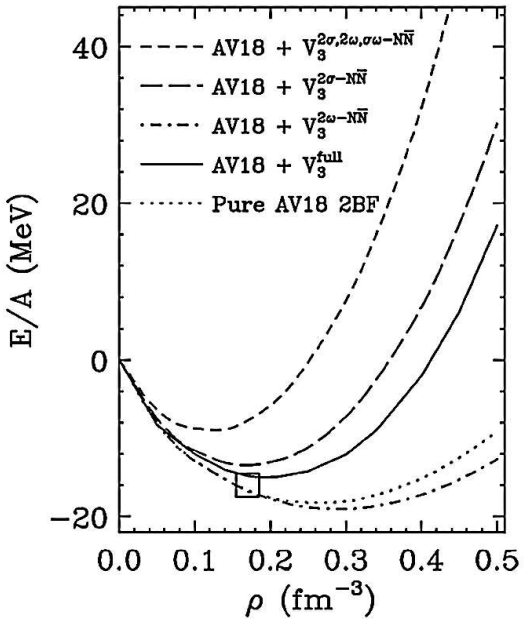

Fig. 1. BHF calculations of the nuclear-matter EOS including three-body forces. The binding energy per nucleon is reported as a function of density [8].

[a] e-mail: bonasera@lns.infn.it

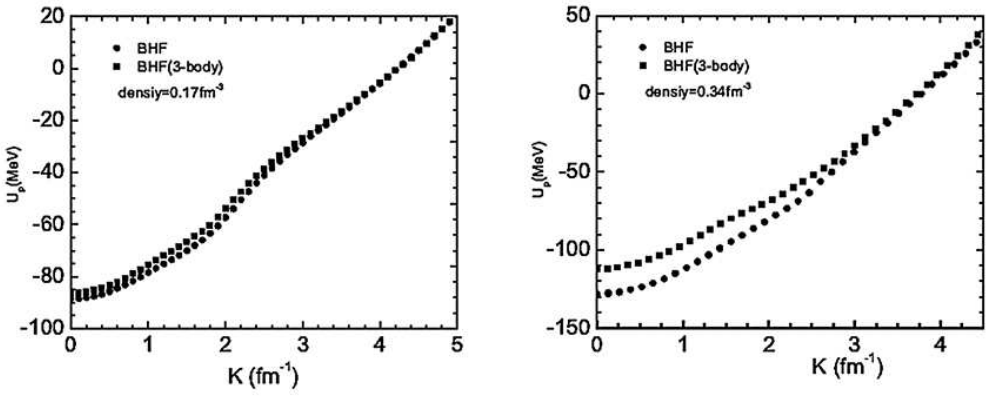

Fig. 2. BHF calculations. The proton potentials are reported as a function of the proton momenta for two different nuclear-matter densities.

ple, that the interplay between two- and three-body forces is very subtle and it turns out that, to fit the ground-state properties of nuclear matter in non-relativistic microscopic calculations, it is necessary to introduce a three-body force [8]. This is demonstrated in fig. 1 for microscopic Bruckner-Hartree-Fock (BHF) calculations [8] where the binding energy per nucleon is reported as a function of the density of nuclear matter at zero temperature. In the figure, the calculations with only two-body forces are given by the dotted line. The two-body force is parameterized to fit the NN data. We clearly see that the approach does not work, in fact it gives a ground-state density of about $0.3\,\mathrm{fm}^{-3}$ and a binding energy of about $-20\,\mathrm{MeV}$, while experimental data correspond to $0.15\,\mathrm{fm}^{-3}$ and $-16\,\mathrm{MeV}$, respectively (square symbol in fig. 1). In order to improve the agreement to data, a genuine three-body force was included in the calculations. The contribution from different channels is displayed in the figure and the final result is represented by the full line. The effect is indeed dramatic. The ground-state density is shifted to $0.19\,\mathrm{fm}^{-3}$ and the binding energy to the experimental value. The three-body force is obtained through a fit to the binding energies of light nuclei, t and ^{3}He essentially [9], but the one reported in fig. 1 is obtained by the meson-exchange model of Fujita-Miazawa [8]. In these nuclear-matter calculations there are no adjusted free parameters. The fact that calculations are not yet perfect implies that something is still missing. Some light on this problem could be shed by experimental data on nucleon production in heavy-ion collisions. We will show below that such data do not support the need for a strong three-body force.

The equation of state discussed so far is at zero temperature. A complete knowledge of the EOS requires, however, information at finite temperatures. Microscopic calculations performed at finite temperatures show, as expected, that the EOS of nuclear matter looks like a Van Der Waals (VDW) EOS. In fact, the NN force has an attractive tail and a repulsive hard core such as many classical systems. At variance with classical systems the ground state is not a solid but a Fermi liquid. However, other properties such as the liquid-to-gas phase transition at finite temperatures and small densities, are of the VDW type [10]. An important feature that makes nuclei different from classical systems is the strong momentum dependence of the mean field. Microscopic BHF calculations give strong indications on how the momentum dependence force should look like in nuclei and nuclear matter. Typical results of non-relativistic BHF calculations are given in fig. 2 where the potential for protons is reported as a function of the nucleon momentum transfer for two different nuclear-matter densities [8]. Also in this case the difference between 2- and 3-body forces is large especially for low momenta and at high densities. Notice the difference between two- and three-body forces at the two different densities. These features might be revealed through a careful analysis near the Fermi energy for the first case and at higher incident energies in the second one.

To study the momentum dependence of the nuclear mean field we have already many findings coming from electron scattering [11]. However, in those experiments the mean field can be only tested at ground-state densities relevant for the results of fig. 2 left panel. At variance, in a heavy-ion collision, depending on the beam energy, higher densities can be explored. The momentum dependence of the force, as well as the compressibility of the EOS might be inferred, or at least strongly constrained, by subthreshold production of pions, gamma-rays and energetic particle emission. Concerning the relevance of NN collisions and in-medium effects on the NN cross-section, effects can be seen in proton experiments [12,13].

In this work, we will restrict ourselves to energies below roughly $100\,\mathrm{A{\cdot}MeV}$, where non nucleonic degrees of freedom (such as Δ excitation) are not so relevant yet. This energy region, we believe, carries important information on the EOS near the ground-state density and moderate temperature. In fig. 3 the maximum and average densities estimated by VUU calculations for central collisions as a function of the incident energies are reported for the $^{40}\mathrm{Ca} + {}^{40}\mathrm{Ca}$ reaction [14]. The understanding of nuclear-matter properties at moderate densities is crucial if we want to understand the EOS at higher densities and temperatures where other degrees of freedom become relevant. In particular, in our contribution we will not discuss

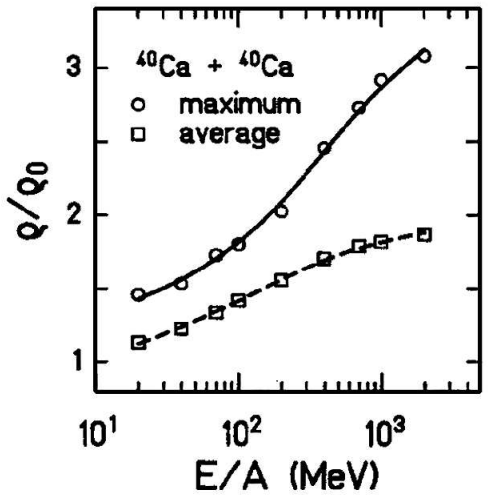

Fig. 3. Maximum and average densities as a function of the bombarding energy per nucleon as estimated by VUU calculations for central ^{40}Ca + ^{40}Ca reactions [14].

the kaon and η production because they require quite a different production mechanism with respect to the one relevant at the lower energies discussed here.

The understanding of the EOS in the region of our interest has to go step by step with the elaboration of microscopic models. While some features of the EOS can be obtained directly from the data, a more quantitative understanding of nuclear properties must be obtained from a detailed comparison between models and data. For instance, we expect that energetic photon and pion production must be very sensitive to the momentum-dependent part of the mean field. In fact, assuming incoherent NN collisions, the final momenta of the colliding nucleons after producing a pion or a photon are decreased. This results in a strong (repulsive) mean field which acts against the production of the new particle essentially because the colliding nucleons must provide an extra energy to overcome the repulsive field. Their final momenta are further reduced and they must not be Pauli blocked, otherwise the collision is not allowed. Unfortunately, we have not been able to find in the literature microscopic calculations of subthreshold particle production with momentum-dependent forces in our region of interest. Many calculations exist for nucleons or more complex particle spectra and as a general feature a reduction of incoherent NN collisions has been found with momentum-dependent forces. Comparison of yields and slopes of energy spectra of energetic protons with predictions of transport models that include a local and a momentum-dependent potential have been published and will be discussed later in this chapter. If one extends this result to subthreshold particle production, a difference of the calculated yield, compared to the results for momentum-independent forces, is expected. This aspect should be carefully (re)analyzed also for π and hard-photon production.

Most of the microscopic calculations, Boltzmann or molecular-dynamics–based [14–17] have two main ingredients. One is the mean field which is parameterized to fit some general results such as electron scattering data, ground-state properties of nuclei etc. The other feature is a collision term which is composed of a probability inferred from NN data, and a Pauli blocking which forbids that particles undergoing an elastic or inelastic scattering, end up in an occupied state. These two ingredients of the models are usually uncoupled, while in principle they should come from the same microscopic interaction. Few attempts exist to date to calculate these ingredients microscopically from the same interaction and to implement them in a transport code (see the contribution by Fuchs and Wolter, *Modelization of the EOS*, this topical issue). In most calculations the phenomenological approach underlined above is used, and one tries to put constraints from a comparison to data. The problem is that most often data are sensitive to both ingredients and it is not easy to disentangle them. However, a systematic comparison of the models to the data should give some constraints on the mean field and the collision term which are included in the calculations.

It is important to stress that in this approach the determination of physical parameters completely relies on the comparison with a transport code, *i.e.* it is fully model dependent. It is, therefore, essential that the different dynamical models and their different numerical implementations within the same parameter set, give compatible results for the observables. The detailed comparison between different codes is an important part of the WCI initiative [18], and tends to show that ambiguities exist among numerical codes, which should be solved before any physical conclusion can be obtained.

Apart from constraining EOS parameters, the interest in studying particle production also relies in the understanding of the production mechanism itself. As we will show in great detail in the following, there are three types of observations:

- particles with an energy much greater than the beam energy in the center of mass. These particles are most likely emitted in cooperative processes that require the collaboration of many nucleons;
- particles with an energy around the beam energy in the center of mass. These particles are presumably created via incoherent processes at the beginning of the reaction when beam particles have still their initial energy;
- particles with an energy much lower than the beam energy in the center of mass. These particles test presumably the late stage of the interaction and may reflect the temperature of the (sub)system.

If this general classification is well established, the transition between the different mechanisms and their detailed modelization are not yet clear and depend on the particle type. For this reason, we have chosen to review particle production according to the particle type.

In the next sections we will discuss some relevant features of data and comparison to models. Indeed, probes of the different stages of the reaction are necessary to achieve a complete picture of the reaction dynamics and to gather information about the EOS of nuclear matter. Energetic

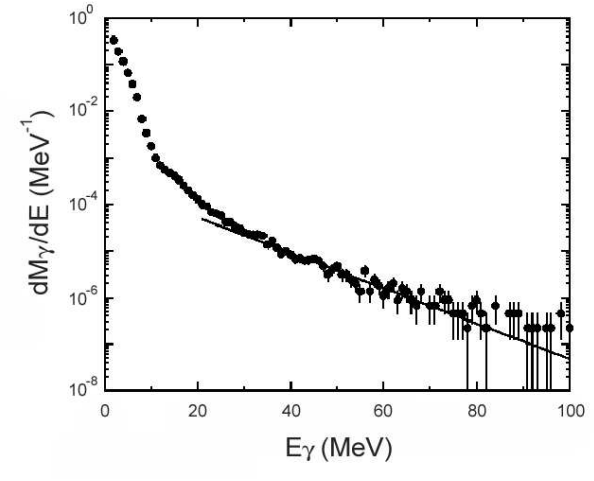

Fig. 4. Gamma multiplicity spectrum for incomplete-fusion reactions in $^{36}\mathrm{Ar} + {}^{98}\mathrm{Mo}$ reactions at 37 A·MeV. The continuous line indicates the exponential fit of the hard component ($E_\gamma \geq 35$ MeV).

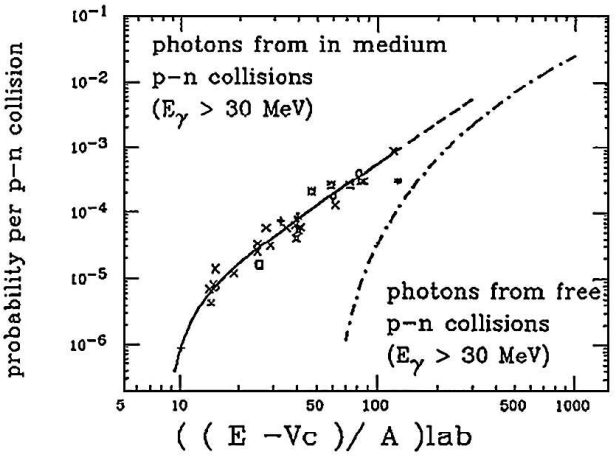

Fig. 5. Emission probability of photons with $E_\gamma \geq 30$ MeV for in-medium NN collisions as a function of the incident energy per nucleon. V_c is the Coulomb barrier [49].

particles like protons, neutrons, pions, and gamma-rays were originally proposed to characterize the initial stage of the reaction. It is clear that energetic photons can do that since their mean free path in nuclear matter is very long, thus once they are produced, they are not scattered again. This is similar for kaons. We have to cite an early experiment at Ganil at 94 A·MeV where kaons were detected [19]. Since then no further data at that energy regime has been discussed, but we believe we have nowadays very performing detectors which could study kaons produced in heavy-ion collisions at around 100 A·MeV. The potential interest of kaons will be clearer after discussing nucleons, pions and hard photons.

2 Hard-photon production

The spectrum of photons emitted in heavy-ion collisions at intermediate energies carries much information on the system evolution from the very early stage of the collision to the late phase at the end of the de-excitation process. Hard photons are particularly appealing probes, since they do not interact again with the surrounding nuclear matter after the production and, therefore, might also provide information on the nuclear-dynamics chronology at various stages of the reaction. A very good review of hard-photon production is given by ref. [14], where the possibility of exploiting energetic particles as probes of the first stages of the reaction is deeply investigated.

A typical spectrum of photons emitted in heavy-ion collisions at intermediate energies is reported in fig. 4 for the reaction $^{36}\mathrm{Ar} + {}^{98}\mathrm{Mo}$ at 37 A·MeV [20]. As a first rough classification we can divide the spectrum in three main regions with increasing energies:

– in the energy range from some hundreds of keV to approximately 10 MeV the spectrum is dominated by the statistical emission from excited nuclei occurring at the end of the de-excitation process;
– in the energy range between roughly 10 MeV and 20 MeV a bump due to the γ decay of the giant dipole resonance (GDR), which is a major isovector collective mode in nuclei, can be observed [21,22]. The γ decay of the GDR has been extensively investigated also in hot nuclei in order to gather information on the maximum temperature that a nucleus can hold [23]. This subject is covered in the contribution *Evolution of the Giant Dipole Resonance properties with excitation energy* by Santonocito and Blumenfeld in this topical issue;
– in the energy range beyond 30 MeV the spectrum is characterized by a large inverse slope parameter increasing with energy and by a yield that, for a given incident energy per nucleon, increases with the size of the colliding nuclei. These high-energy gamma-rays ($E_\gamma \geq 30$ MeV) are the so-called hard photons, and are the subject of this part of our review. Their production has been deeply investigated. The main results will be reported in the following with the current understanding of the hard-photon emission and open problems which still need further investigations.

The first experimental observation of an unexpected hard component in the photon spectrum emitted during nucleus-nucleus collisions was found in the $^{12}\mathrm{C} + {}^{12}\mathrm{C}$ reaction at 84 A·MeV. This experiment aimed at the study of subthreshold neutral pions π^0's, which decay by the emission of two energetic photons, hard photons representing a background [24]. The analysis of these first data [25] revealed many interesting features from both the experimental and theoretical point of view. Indeed, in spite of the very low hard-photon cross-section, several (inclusive) experiments followed with various projectile-target combinations on a rather broad energy range between 10 A·MeV [26] and 124 A·MeV [27]. Indeed hard photons are expected to be a good probe up to 90 A·MeV, since at

higher incident energies the contributions of the π^0 decay cannot be neglected (see fig. 5 and fig. 10).

Inclusive experiments yield information about hard-photon cross-sections, inverse-slope parameters, angular distributions and source velocities. From a theoretical point of view, the question about the origin, *i.e.* the production mechanisms, of hard-photon emission was also faced and the proposed solutions can be summarized as follows:

- nucleus-nucleus collective bremsstrahlung [28–30] where photons are emitted as a consequence of the coherent deceleration of the electric field of the two colliding nuclei. The photon yield strongly increases with increasing energy and the spectrum slope depends on the deceleration time;
- incoherent bremsstrahlung as a consequence of NN, in particular n-p, collisions occurring in the interaction region in the first stages of the reaction [31,32], as radiation due to proton deceleration. Several prescriptions have been used for the np-$np\gamma$ cross-section such as the semi-classical one [33], the neutral scalar meson exchange model, and others [34,35]. If these prescriptions are sometimes contradictory, the situation is presently largely clarified after the results of recent experiments which studied the proton-induced reactions at 190 MeV on a liquid-hydrogen target [36]. In this experiments high p-p bremsstrahlung data have been obtained. Moreover, studies on a deuterium target [37, 38] have allowed to investigate all the channels leading to gamma bremsstrahlung, including the coherent bremsstrahlung contribution;
- statistical emission either from a compound-like emission [39] or from a "fireball"-like system [40], where the spectrum slope should reflect the temperature of the emitting source;
- cooperative effects where several nucleons group together into virtual clusters which provide the extra energy for the hard-photon production [41].

The inclusive data systematics gave evidence of a source velocity close to half the beam velocities and an angular emission pattern consistent with an isotropic plus a dipole-like emission in the source reference frame [14]. These results are consistent with the n-p bremsstrahlung mechanism as a dominant process in the hard-photon emission in heavy-ion collisions at intermediate energy. The absolute yield is however much larger than expected from free n-p collisions, and this difference strongly increases with decreasing beam energy. For this reason, hard photons are considered as "subthreshold particles" using the same definition that applies for mesons produced at an incident energy per nucleon lower than the energy threshold for free NN collision. This feature has been successfully explained in terms of the Fermi boost provided by in-medium nucleon-nucleon collisions (see fig. 5).

Alternative approaches have also been proposed. In particular, some results have been rather well reproduced by a statistical approach, *i.e.* the experiments ^{92}Mo + ^{92}Mo at 19 A·MeV [39] and N + (C, Zn, Pb) at 20, 30 and 40 A·MeV [42]. However, it is important to mention that hard-photon angular distributions in asymmetric systems [43,44] are consistent with a source velocity close to half the beam velocity with the presence of a dipole component, rather than to the compound nucleus velocity.

The unique result indicating evidences of coherent bremsstrahlung [45] was not confirmed. Anyway, the expected yield for collective nucleus-nucleus bremsstrahlung [29] is much lower than the observed ones. Dynamical calculations indicate that at most 10% of the observed hard-photon ($E_\gamma \geq 50$ MeV) [31] cross-section is consistent with nucleus-nucleus bremsstrahlung, while the dominant part of the total yield is due to first chance n-p collisions. It is important to note, however, that inclusive data are also consistent with n-p bremsstrahlung in a nuclear fireball.

In order to disentangle the different hypotheses concerning the origin of the hard-photon emission and to get a deeper insight on the phenomenon, exclusive measurements were necessary. A first group of measurements faced the issue of the impact parameter dependence of the hard-photon production. The first experiments indicated that the hard-photon multiplicity increases with increasing reaction centrality and the slope slightly decreases with increasing impact parameter [42,46–48]. These experimental facts are, unfortunately, again well accounted for by different theoretical models. In the fireball model [40], the hard-photon multiplicity scales with the volume of the interaction zone, which increases with increasing centrality. In dynamical calculations like BUU [31], where hard photons ($E_\gamma \geq 50$ MeV) are mostly emitted as a consequence of first n-p collisions, a hard-photon multiplicity dependence on the overlap of target and projectile nuclei is found consistent with emission in the first stages of the reaction [31]. Moreover, in dynamical calculations, the decreasing of the slope with increasing impact parameter is interpreted as due to the fact that nucleons with softer momentum are mostly located at the nuclear surface.

The quality of exclusive data was strongly boosted by the high efficiency of two multidetector apparatuses for hard photons, MEDEA, by which hard photons and light charged particles can be detected simultaneously [1], and TAPS [5]. In particular, the dependence of hard-photon multiplicity M_γ on the impact parameter b was investigated quantitatively. In models based on n-p bremsstrahlung, the hard-photon multiplicity scales with the number of n-p collisions (N_{np}) and therefore with the size of the interaction zone (A_{part}):

$$M_\gamma(b) = P_\gamma \cdot N_{np}(b) \propto P_\gamma \cdot A_{part}(b).$$

Here P_γ is the probability of emitting a hard photon in a single n-p collision (p-p collisions are not considered since they provide a much smaller contribution $\leq 10\%$) at a given incident energy for a heavy-ion reaction. This probability is usually extracted from inclusive data (see [49] for systematics) within the approximation that P_γ in nuclei only depends on the incident energy per nucleon. Several experiments [50–52] were run and compared with the results of dynamical models based on a transport equation to simulate nucleus-nucleus collisions, whereby the

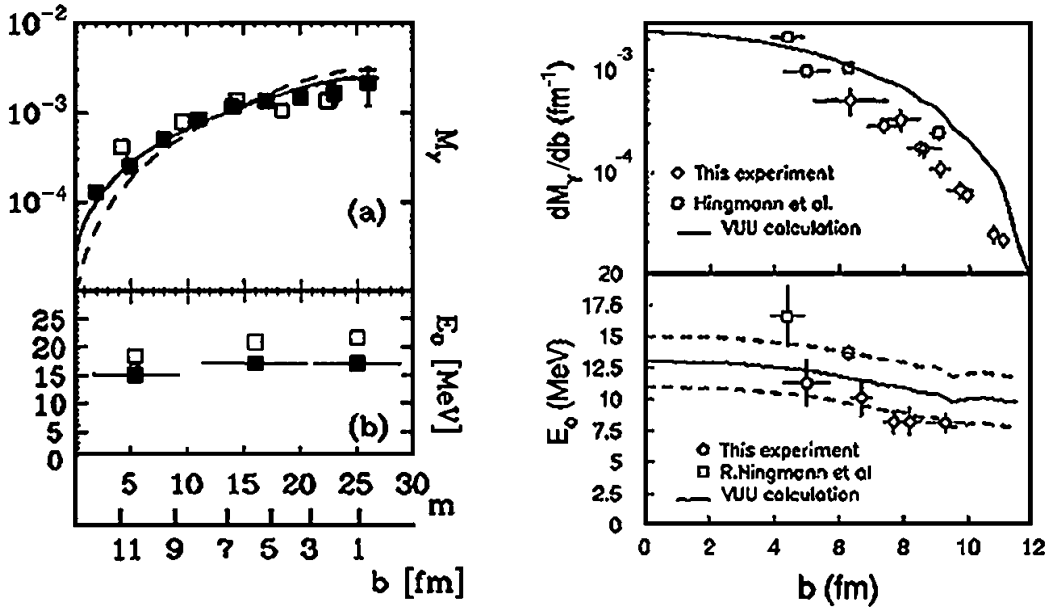

Fig. 6. Gamma-ray multiplicity for $E_\gamma \geq 40\,\mathrm{MeV}$ (left top panel) and for $E_\gamma \geq 25\,\mathrm{MeV}$ (right top panel) and inverse-slope parameters (bottom panels) as a function of the centrality for the reaction Xe + Au at 44 A·MeV (solid squares in the left panels, ref. [51]) and for the reaction Ar + Gd at 44 A·MeV (open symbols in the right panels, ref. [50]). In the left panels, for comparison, BNV calculations are reported (open symbols) while the continuous line is calculated assuming M_γ proportional to the surface of the overlap zone and the dashed line is calculated assuming M_γ proportional to the volume of the overlap zone. In the right panels VUU simulations are reported (full lines, dashed lines are the uncertainties).

hard-photon production is treated in a perturbative way. In fig. 6 the measured and calculated M_γ and inverse-slope parameters as a function of the estimated impact parameters are reported for two different reactions measured with two different apparatuses. In general, a rather good qualitative agreement between the measured and calculated hard-photon multiplicity for several reactions is observed. Moreover, the γ-ray multiplicity appears to scale with the surface of the overlap region in the reaction $^{129}\mathrm{Xe} + {}^{197}\mathrm{Au}$ at 44 A·MeV (see fig. 6 top left panel). For the same reaction a good agreement with BNV calculation was found [51]. These results provide a further support for the models based on *n-p* bremsstrahlung. Similar information was gathered from inclusive data varying the size of the colliding nuclei. Eventually, these experimental data provide a measurement of the spatial origin of the hard photons from the interaction zone. It is important to underline the fact that the hard-photon multiplicity scales linearly with the participant region, does not necessarily imply that a fireball is formed as an independent source, but, especially around the Fermi energy, rather provides a snapshot of the interaction zone in the early stage of the reaction. For this reason the hard-photon multiplicity can also be used as a quantitative measure of the impact parameter in heavy-ion collisions.

This large set of data, although consistent with BUU calculations, cannot rule out a fireball scenario especially at the higher incident energies. For this reason, a deeper insight into hard-photon production was attempted by looking at hard-photon–particle correlations and hard two-photon correlations. In calculations in which hard photons mainly arise from first chance *n-p* collisions, if the photon and proton energies are high enough, an anticorrelation is expected due to the kinematical limit imposed on the total proton and gamma-ray energy in the bremsstrahlung process. In the reaction $^{14}\mathrm{N} + \mathrm{Zn}$ at 40 A·MeV the gamma-ray proton coincident ratio was found to be independent of proton energy for $E_\gamma \geq 20\,\mathrm{MeV}$, thus suggesting that high-energy photon production, for $E_\gamma \geq 20\,\mathrm{MeV}$, may arise in part from *n-p* bremsstrahlumg in a later stage of the collision [53]. On the other hand, high-statistics data on the reaction $^{40}\mathrm{Ar} + {}^{51}\mathrm{V}$ at 44 A·MeV [54] were also analyzed. These data show that, while hard photons with $E_\gamma \geq 25\,\mathrm{MeV}$ exhibit a slight anticorrelation constant with increasing energy, the very energetic photons, namely with $E_\gamma \geq 70\,\mathrm{MeV}$, exhibit a much stronger anticorrelation increasing with increasing proton energy as expected in a first chance *n-p* bremsstrahlung scenario. This result, which confirms the expectations of dynamical models (see [14]), provide an experimental evidence of the hypothesis that very energetic photons are mostly produced in the early stage of the reaction. This signature qualifies high-energy photons (as well as protons) as probes of the momentum and energy distributions of the nucleons in the early stages of heavy-ion collisions. Hard two-photon correlations were investigated in different systems, and the results reported in refs. [55,56] also support the idea that hard photons originate from an early stage of the reaction.

Besides the understanding of the production mechanism, the study of the hard-photon emission allows to use them as probes of the nuclear matter. In particular,

due to the nature of the electromagnetic radiation, they can carry unperturbed information on the nuclear matter at the moment of their production and are not affected by subsequent stages of the reaction. Information on nuclear dynamics, on the contribution of the mean field and two-body collisions in dissipative heavy-ion reactions, and a time scale for multifragmentation have been deduced by detailed investigation of the hard-photon emission in heavy-ion collisions at intermediate energy and the main results are reviewed in the following.

In collisions around the Fermi energy, the nuclear dynamics is governed by the interplay between one- and two-body dissipation, namely between the mean-field and NN collisions. At energies around and above the Fermi energy (about 35 MeV) the role of NN collisions increases with increasing incident energy due to a reduced contribution of the Pauli blocking, which inhibits NN collisions at low energy. Two different experiments addressed the problem of one- and two-body dissipation mechanisms at intermediate energy via the study of hard-photon emission in peripheral and central reaction, respectively. Hard photons were measured in coincidence with projectile-like fragments in the reaction $^{36}\mathrm{Ar} + {}^{159}\mathrm{Tb}$ at 44 A·MeV in the peripheral events [57]. The hard-photon multiplicity, which scales with the number of *n-p* collisions, as discussed above, and therefore represent a measure of two-body dissipation, was measured as a function of the mass of the primary projectile-like mass and was found to increase linearly with the transferred mass, showing the importance of two-body collisions. Moreover, the multiplicity value depends on the direction of transfer. Indeed more collisions are needed to transfer mass from the heavier target than viceversa; this effect is understood in terms of the action of the mean field that favors nucleon transfer from the lighter to the heavier partner of the collision. A complementary study for central collisions leading to incomplete-fusion residues was reported in ref. [58]. In this case, hard photons ($E_\gamma \geq 35$ MeV) were measured in coincidence with heavy residues emitted in the reactions $^{36}\mathrm{Ar} + {}^{90}\mathrm{Zr}$ at 27 A·MeV and $^{36}\mathrm{Ar} + {}^{98}\mathrm{Mo}$ at 37 A·MeV. In this incident energy regime, central and semi-central collisions lead to incomplete fusion and this process is usually described by the Viola systematics that shows a decrease of the momentum transfer as a function of the incident energy [59]. In the two ^{36}Ar-induced reactions cited above, the ratio between the residue velocity and the center-of-mass velocity (v_r/v_{cm}) was measured as a function of the reduced impact parameter (b/b_{max}) given by the hard-photon multiplicity. A strong correlation is found between v_r/v_{cm} and b/b_{max}. Most remarkable, data coincide for both incident energies. This indicates that the fraction of linear momentum transfer for events giving rise to a residue depends only on the impact parameter and not on the bombarding energy. This demonstrates the role of two-body collisions in the transfer process leading to the production of highly excited nuclei. In conclusion, the hard-photon detection has played an important role in elucidating the interplay between mean-field and NN collisions around the Fermi energy both in peripheral and central collision, leading respectively to projectile-like fragments (PLFs) and heavy residues.

High-energy photons do not only probe the first stage of the collision. A contribution from a second, less energetic, photon source emitted in a later phase of the reaction was put in evidence in several reactions at various incident beam energies. The feature of this so-called "thermalized" hard-photon component and its consistency with statistical and dynamical model calculations are discussed in the following.

Hard photons ($E_\gamma \geq 30$ MeV) were measured in the reactions induced by an ^{36}Ar beam at 95 A·MeV on ^{197}Au and ^{12}C. It is important to note that in this case the incident energy per nucleon is well above the free NN threshold for the production of photons with $E_\gamma \geq 30$ MeV. It was shown [54] that while very energetic photons originate from the first phase of the reaction, the bulk of photons ($E_\gamma \geq 30$ MeV) is produced over a longer time span and could probe if the phase that leads to the thermalization of the fireball is formed in the reaction [60]. From an experimental point of view, the very good statistics hard-photon measurements with the MEDEA [1] and TAPS [5] detectors demonstrate that a good description of hard-photon spectra is obtained with the superposition of two components with different slopes and yields[1]. Moreover, hard two-photon interferometry measurements in the reactions $^{86}\mathrm{Kr} + {}^{nat}\mathrm{Ni}$ at 60 A·MeV and $^{181}\mathrm{Ta} + {}^{197}\mathrm{Au}$ at 39.5 A·MeV are well described within the hypothesis of two different sources [61]. The softer component has been associated with photon emission in a later stage of the reaction. In BUU calculations, besides the dominant hard-photon contribution produced by *n-p* bremsstrahlung during the compression phase at the early stage of the reaction ("direct" photons), "thermal" hard photons are also emitted in a later stage from less energetic *n-p* collisions inside a thermalized source during the resilience of the system after the expansion phase. Experimentally, inclusive and exclusive photon spectra consistent with a "thermal" and a "direct" component were measured in the reactions $^{86}\mathrm{Kr} + {}^{nat}\mathrm{Ni}$ at 60 A·MeV, $^{181}\mathrm{Ta} + {}^{197}\mathrm{Au}$ at 39.5 A·MeV, $^{208}\mathrm{Pb} + {}^{197}\mathrm{Au}$ at 29.5 A·MeV [62] and in the reactions $^{36}\mathrm{Ar} + {}^{197}\mathrm{Au}$, $^{107}\mathrm{Ag}$, $^{58}\mathrm{Ni}$ and $^{12}\mathrm{C}$ at 60 A·MeV [63] and in the reactions $^{58}\mathrm{Ni} + {}^{27}\mathrm{Al}$, $^{58}\mathrm{Ni}$ and $^{197}\mathrm{Au}$ at 30 A·MeV [64] and $^{58}\mathrm{Ni} + {}^{197}\mathrm{Au}$ at 45 A·MeV [65–67].

An appealing aspect of thermal photons is that their emission signals that a big piece of nuclear matter still exists at the end of the dynamical evolution of the collision, and their slopes can be related to the temperature of such a system. This can be exploited to get information on other processes using thermal photons as a probe. For instance, the nuclear caloric curve has been investigated using thermal photons as a new "thermometer" for hot nuclear matter [68]. Moreover, thermal photons have been used as a "clock" to deduce the time scale of intermediate mass fragment (IMF) emission. Studying the

[1] However, we would like to notice that the change in slope of the photon yield could be also affected by the $1/E_\gamma$ factor which enters the elementary np-$np\gamma$ bremsstrahlung probability [15].

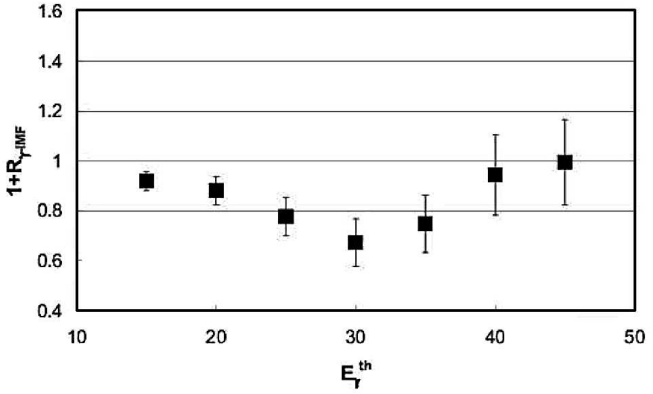

Fig. 7. Experimental photon-IMF correlation factor *versus* the threshold E_γ for IMFs in the velocity window near the center-of-mass velocity. Data are shown for the Ni + Au reaction at 45 A·MeV for central collisions.

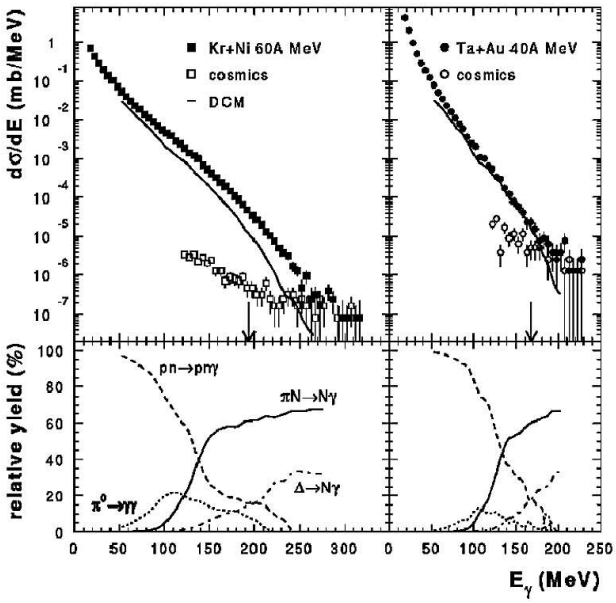

Fig. 8. Measured photon spectrum (full symbols) in the reaction ^{86}Kr + ^{nat}Ni at 60 A·MeV (left panel) and ^{181}Ta + ^{197}Au at 40 A·MeV (right panel) after subtraction of the cosmic-ray contribution (open symbols). The solid line represents calculations. In the lower part, the calculated spectrum is decomposed into fractions corresponding to the following mechanisms: $pn \to pn\gamma$, $\pi N \to N\gamma$, $\pi^0 \to \gamma\gamma$, $\Delta \to N\gamma$ [69].

thermal photon-IMF correlations, an anticorrelation signal with IMFs in the nucleus-nucleus center-of-mass velocity region has been observed in central Ni + Au collisions at 45 A·MeV (fig. 7) [66], while the same has not been seen in the data for the same system at 30 A·MeV [67]. This indicates that around 45 A·MeV a transition occurs from late to prompt IMF emission, where "prompt" has to be interpreted as faster than the emission time associated with thermal photons. Stochastic mean-field simulations performed for these two reactions are consistent with the data. At 30 A·MeV for most of the events the system, after the initial compression and expansion, recombines leading to the formation of an heavy excited system with $Z \approx 80$. On the other hand, at 45 A·MeV a dominant role of a prompt IMF formation is observed [65,66].

The last part of the γ-yield concerns the very high-energy part of the spectrum. Deep sub-threshold particles, with respect to the kinematical limit expected for NN collisions including the boost due to the Fermi motion, are observed on a broad range of incident energies addressing the question of which mechanism allows to concentrate such a relevant fraction of the total available energy in the production of a single energetic or massive "particle". Several hypotheses have been considered such as nucleon off-shell effects, three-body collisions, dynamical fluctuations or multi-step processes involving pion and Δ's.

High-statistics data exhibit the presence of hard photons with energy well above the kinematical limit for NN collisions. In the reactions ^{86}Kr + ^{nat}Ni at 60 A·MeV and ^{181}Ta + ^{197}Au at 40 A·MeV [69], hard-photon spectra, with energy extending up to 5 times the beam energy per nucleon, were measured. The data were compared with a cascade model which takes into account several channels (see fig. 8) including the radiative channel $\pi + N \to N + \gamma$. The calculations are in good agreement with the data for the reaction ^{181}Ta + ^{197}Au at 40 A·MeV, while undershoot the data of the reaction ^{86}Kr + ^{nat}Ni at 60 A·MeV, both concerning the highest-energy component of the photon spectrum and slope and yield of the π^0 energy spectrum. In summary, theoretical calculations, in spite of the many hypotheses proposed, are not satisfactory in explaining deep subthreshold data and a more detailed comparison between data and models is desirable. We will come back to the problem of deep subthreshold particle production in the next section, devoted to pions.

3 Subthreshold pion production

Pions (and nucleons), at variance with photons, after being produced, can interact with nuclear matter again and be scattered and/or reabsorbed. These multiple interactions of pions with the surrounding matter explain the early success of statistical models [70–72]. On the other hand, rescatterings lead to ambiguities in transport approaches where pion production is calculated perturbatively, similarly to hard photons. This method is in principle not applicable because pion dynamics should be followed microscopically. What is generally done in the literature is to correct the results with an absorption factor expressed in terms of a pion mean free path, and in turn obtain a value for the mean free path for each experimental condition [14–16,73,74]. For this procedure to be fully consistent, the other parameters entering the calculation should be fixed from independent observables, for instance, photon production in the same reaction. Unfortunately, this is rarely reported in the literature we are aware of.

Keeping this problem in mind, in this section we would like to review some of the experimental data on pion pro-

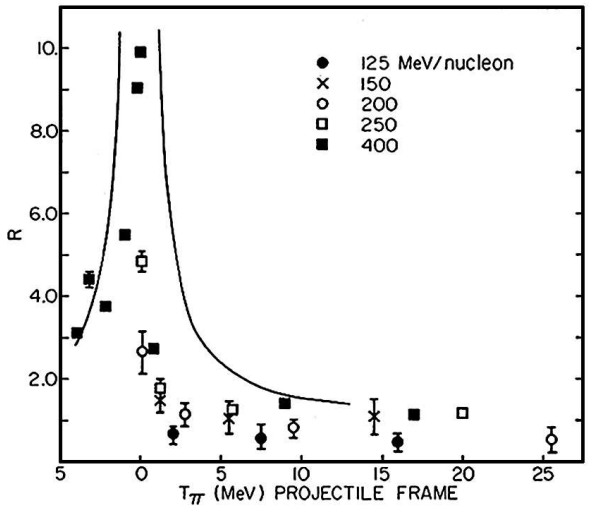

Fig. 9. Ratio R of π^- to π^+ cross-section in Ne + NaF at different incident energies as a function of the pion energy in the projectile frame. The solid curve shows the Coulomb energy as described in the text [75].

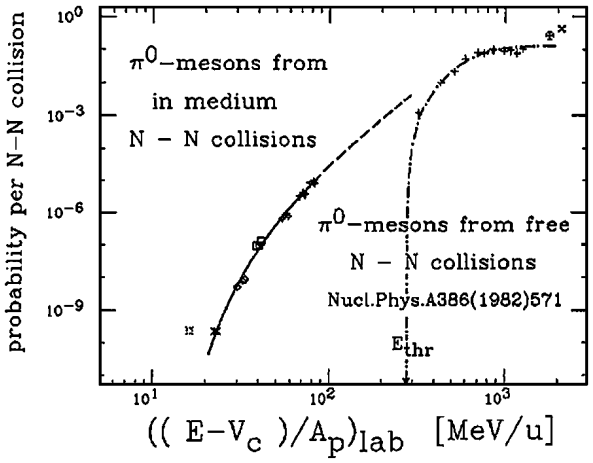

Fig. 10. Emission probability of neutral pions for in-medium NN collisions as a function of the incident energy per nucleon. V_c is the Coulomb barrier [14].

duction at energies ranging from the absolute kinematical threshold to about 100 A·MeV. An abundant literature on higher energies exists, which is however outside the scope of this work.

First data on pion production at subthreshold energies (corresponding to a beam energy per particle in the laboratory below twice the pion mass) were obtained by Benenson *et al.* at LBL above 100 A·MeV [75] and subsequently at much lower beam energies, ^{16}O + Al, Ni at 25 A·MeV [76]. The latter result was somehow surprising, at that time, because one would estimate a higher threshold for pion production around 50 A·MeV by coupling the relative to the Fermi motion in first-chance NN collisions. In the work of Benenson *et al.* the ratio of π^+/π^-, reported in fig. 9, was measured and successfully explained in terms of a statistical model which invoked the ratios of the absorption cross-sections and a Coulomb shift (see the full line in fig. 9) [72].

A collection of available data was analyzed in terms of probability of elementary NN collisions folded with the number of possible collisions in a nucleus-nucleus interaction. This gave a scaling approximation similar to the one reported for photon production, which is displayed in fig. 10 [46,49]. This scaling shows that at least the gross features could be understood in terms of single NN collisions. Below, we will show that this mechanism is however insufficient to explain data very close to the kinematical threshold.

To enter more in detail into the microscopic calculations, we briefly recall how pion production is simulated in kinetic models. This is very similar to photon production discussed above, *i.e.* for each elementary NN collision the production probability is calculated perturbatively. This means that for each elementary collision a pion of a given charge (charge conservation enforced) and energy is produced according to an emission probability extracted from a parametrization of the free $NN \to NN\pi$ cross-section. This cross-section is dominated by the excitation of a Δ-resonance as a doorway state. The underlying hypothesis is the neglect of the finite Δ lifetime. The emission angles are randomly chosen and the final momenta of the nucleons are calculated to conserve total energy and momentum in the collision. The obtained probability is multiplied by the Pauli-blocking factors $(1-f)\cdot(1-f)$ for each chosen emission angles of the pion (and averaged over the different emission angles). This approach has been used by many authors [14–16], but one different idea was proposed by W. Bauer in ref. [73]. There it was assumed that pions may be produced through a Δ-resonance whose decay would be hindered by the blocking effect of the Fermi sea. The crucial point for this scenario is to get some information on the mean field seen by Δ's. In fact, if Δ's see a strong repulsive mean field, their formation will not be favored and the process discussed above will be unphysical. Gathering some information about the properties of the mean field seen by the Δ at moderate densities and temperatures could be possible through a careful experimental and theoretical analysis of pion and photon production in the nucleus-nucleus collisions. This would call for a second campaign of coincidence experiments with more performing detectors to study the Δ propagation in the medium supported by a deep theoretical analysis with more recent and refined models that are now available. Since in the world there are many laboratories able to deliver beams of high quality at the energies of interest and there are very good and performing detectors that with small modifications could be suitable to study the type of physics discussed here, there is no need for large financial efforts and to leave the field not fully explored would be a real pity. But in order to disentangle the main features we have understood so far and the questions still not answered, we will go in more detail into the results that have been obtained.

In terms of microscopic models, the first ingredient to be considered is the ground-state momentum distribu-

tion. In the first codes this distribution was given within a degenerate Thomas-Fermi approximation, *i.e.* for each local density a Fermi momentum was calculated and the particles (usually test particles in a Boltzmann transport equation) randomly distributed as a step function with the corresponding local Fermi momentum. This approach lacks self-consistency and the high-momentum tail of the distribution is neglected [14–16]. More recent approaches such as Fermionic molecular dynamics (FMD) [77], antisymmetrized molecular dynamics (AMD) [78], constrained molecular dynamics (CoMD) [79] and more recent Vlasov approaches [80,81] calculate in a self-consistent way the ground state used for the time evolution of the collisions. However, detailed calculations for pion production within the framework of those more refined models are not available to our knowledge.

In the old calculations a large dependence of the pion production on the Fermi momenta was observed. We notice in passing that if the nuclear ground state is not obtained self-consistently, one can change the Fermi energy by modifying slightly the surface term or the momentum-dependent part of the potential (or some parameters of the Gaussian or delta test particles) keeping the nuclear binding energy unmodified. Changing the Fermi energy will change the pion distributions by orders of magnitude [15]. The use of a realistic correlated ground-state momentum distribution fitted from electron scattering experiments [14] naturally allows to increase the maximal Fermi boost, and consequently decrease the threshold energy for pions and all other subthreshold particles. It is, however, worth mentioning that, from a numerical point of view, the particle production rate is not entirely trustable in this approach. Indeed, due to the semiclassical nature of the simulation, test particles initialized in the high-energy tails are not Pauli blocked and may lead to a spurious production of particles already in the ground state. Because of this ambiguity, the question whether energetic particles are produced in incoherent NN encounters or not is not completely solved. Recent data on proton production as a function of the number of participant nucleons [13] clearly demonstrate that cooperative processes have to be invoked when detecting protons whose energies are close to the NN kinematical limit. Similar exclusive data at the energies of interest here and for pion production are unfortunately not available to our knowledge. This kind of data would provide more precise information on the type of mechanism responsible for pion and more general particle production near the kinematical threshold. Furthermore, they will give a more stringent test to the more refined models available nowadays.

As discussed in the introduction, one of the main motivations in studying energetic particle production is the possible sensitivity to the characteristics of the nuclear EOS properties and in-medium cross-sections. Information on these issues coming from pion production is discussed below. The nucleon-nucleon cross-section appears in transport models in the collision term. Most calculations include a two-body collision term which takes into account, in a semiclassical way, the effect of Pauli blocking. However, when the density and temperature of the system increase Pauli blocking relaxes and the dilute-gas approximation which is the basis of the Boltzmann collision term is no longer valid. Attempts have been made to include three-body collisions [82–84] to calculate not only particle production and collective effects [83] but also more complex particle production [84].

It is important to notice that the 3-body collision term is not unique and its expression depends on the adopted approximation scheme [82–84]. In [82,84] a 3-body collision can happen if the particles did not undergo a 2-body collision while in [83] the probabilities for two- and three-body collisions are calculated independently. This latter assumption leads to a decrease of the particle mean free path while the previous one does not necessarily. The two approaches give different values for physical observables such as collective flow under fixed conditions for the other parameters, *i.e.* same elementary NN cross-section and similar mean fields. To discriminate between different treatments, codes should be confronted with analytical solutions accessible in model cases [83], and independent observables sensitive to the nucleon mean free path such as nuclear stopping, should be systematically compared to experimental data. In any case, when three-body collisions are included energetic particles are produced with higher probability as compared to the two-body case and with higher energy [15].

Another important physical ingredient is the nuclear mean field. Many calculations have shown a modest sensitivity to the compressibility of the EOS for pion and photon production. This has been explored especially for momentum-independent interactions. Of course, it is well known that the mean field is momentum dependent (fig. 2) thus models should take into account this feature also for particle production. When the momenta of two (or three) colliding nucleons change because of the scattering, the field changes as well because of its momentum dependence. What one does in practical calculations is to modify the momenta of the particles in such a way that the total energy is conserved. If this is not possible the collision is rejected. This generally results in a reduced number of NN collisions and possibly in a global transparency effect as compared to calculations with momentum-independent forces. The role of the momentum-dependent force should be further investigated when a particle, a pion or a photon is produced. In such a case the final momenta of the nucleons are further reduced because some energy and momentum is carried away from the produced particles. Thus, on top of the Pauli-blocking effect one should consider the effect of the momentum-dependent mean field which being usually repulsive will result in a need for more energy to produce a particle and in turn to a reduction of its formation probability. No microscopic models with momentum-dependent forces that calculate subthreshold particle production are available to our knowledge. Some exist at higher energies where the calculations are non-perturbative [85] and a sensitivity to the EOS is demonstrated. Even in the perturbative regime, calcula-

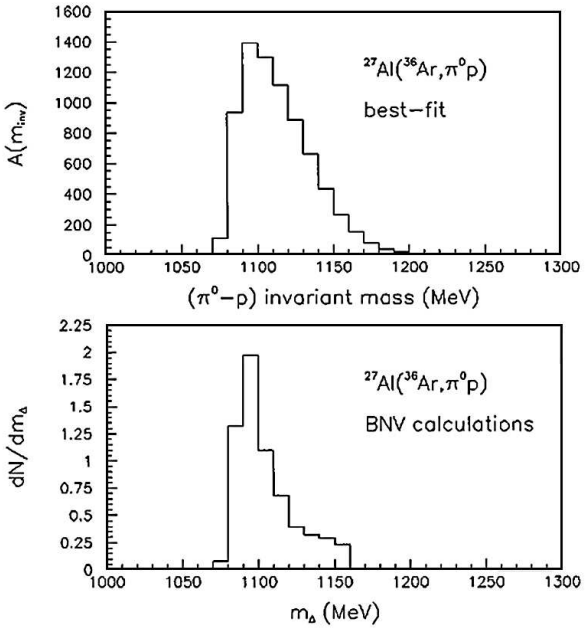

Fig. 11. Comparison between the "indirect" channel (π^0-p) invariant-mass distribution $A(m_{inv})$ (upper panel), extracted from a best-fit procedure, and Δ mass distribution (lower panel) predicted by the BNV theoretical calculation for the same system at the same bombarding energy [86].

tions should be feasible nowadays with the more performing computers.

For the particular case of pion production, if the process occurs through Δ formation and if the Δ cannot decay because of the Pauli principle until it is in vacuum (or in a low-density and high-temperature region), one could try to study the properties of the mean field seen by the Δ. Some experimental data on Δ production in nucleus-nucleus collisions at energy below 100 A·MeV have been discussed in [86,87] and investigated in BNV calculations (see fig. 11). Data show that the Δ width is reduced from its free value to about 25–50 MeV. Naively this would indicate that the Δ lifetime in matter is increased to about 10 fm/c which could be a sufficient time to say that the delta does not decay before the nuclei disassemble. On the other hand, the width of the resonance is roughly reproduced in the BNV calculation as due to the folding of the delta width in vacuum and energy conservation (or Pauli blocking) that blocks the higher-momentum part of the pion distribution. The model has the features discussed above, *i.e.* momentum-independent mean field, Fermi-gas approximation for the initial distribution and two-body collisions only. A more refined approach and more data for other systems at different energies would be needed to study the dynamics of Δ's in moderately excited nuclear matter.

4 Energetic light-particle emission

Together with pions and hard photons, energetic nucleons are a powerful probe to get information on the initially compressed nuclear phase and on the following dynamics, because their emission drives the system towards an expanded and more thermalized stage or a fragmentation stage. Moreover, the knowledge of the energetic particle multiplicities and of the energy dissipated in the first reaction phase is of particular interest for the understanding of the role of the isospin degree of freedom in nuclear reactions and in the EOS for asymmetric nuclear matter.

Energy spectra of light particles ($p, d, t,$ He) have been measured for a large variety of reactions in a wide range of incident energies with apparatuses covering the whole angular range. In fig. 12 the experimental proton energy spectra (dots) for ^{64}Zn + ^{92}Mo collected at different incident energy and detection polar angles measured with the NIMROD apparatus [3] are reported. A frequently used technique to study light-particle emission mechanisms is a simultaneous fit (in energy and in angle) of these spectra assuming isotropic emission from sources with a Maxwellian spectrum in their center of mass. Such analysis performed on energy spectra, collected in inclusive [88–93] data and in data sorted as a function of centrality, [94–97] shows that the procedure is able to give a qualitative characterization of the light-particle emission process.

The source velocities (v_s), the inverse-slope parameters (T), the multiplicities (M) and the Coulomb emission barriers (E_c) are the fit parameters. A good reproduction of the experimental data, in the whole angular range, is possible only if three sources are taken into account: a projectile-like source (PLF) ($v_s \approx v_{beam}$) that dominates at forward angles, a target-like source (TLF) ($v_s \approx 0$) localized at low energies, and an intermediate-velocity source (IS) ($v_s \approx v_{beam/2}$) that dominates at high energies and at larger polar angles. The relative yields of the sources depend on the system asymmetry, on the reaction centrality and incident energy [95,96]. The values of the inverse-slope parameters (T) are of the order of 4–6 MeV for TLF and PLF while, for the IS source, T is much higher, depending on the incident energy. The presence of these three sources is clearly evidenced also in the Lorentz-invariant differential cross-section plots for light particles [95,98].

Light particles emitted from TLF and PLF sources are interpreted as particles evaporated from equilibrated systems with a statistically predicted Maxwellian spectrum. Such interpretation is strengthened by the analysis at lower bombarding energy and/or excitation energies. The exponential slope T reflects the "apparent temperature" of the emitting systems averaged over the whole de-excitation cascade. Applying corrections using statistical models, it is possible to estimate the initial temperatures, that are in agreement with the values estimated with other methods [99].

Protons and neutrons emitted from a source with half beam velocity (IS), which accounts for the most energetic part of the spectra at around 90° in the nucleon-nucleon reference frame, are interpreted as emitted in a non-equilibrated phase of the reaction as a consequence of NN collisions. In ref. [100] mid-velocity emission is already found at 25 A·MeV while the onset of hard-photon

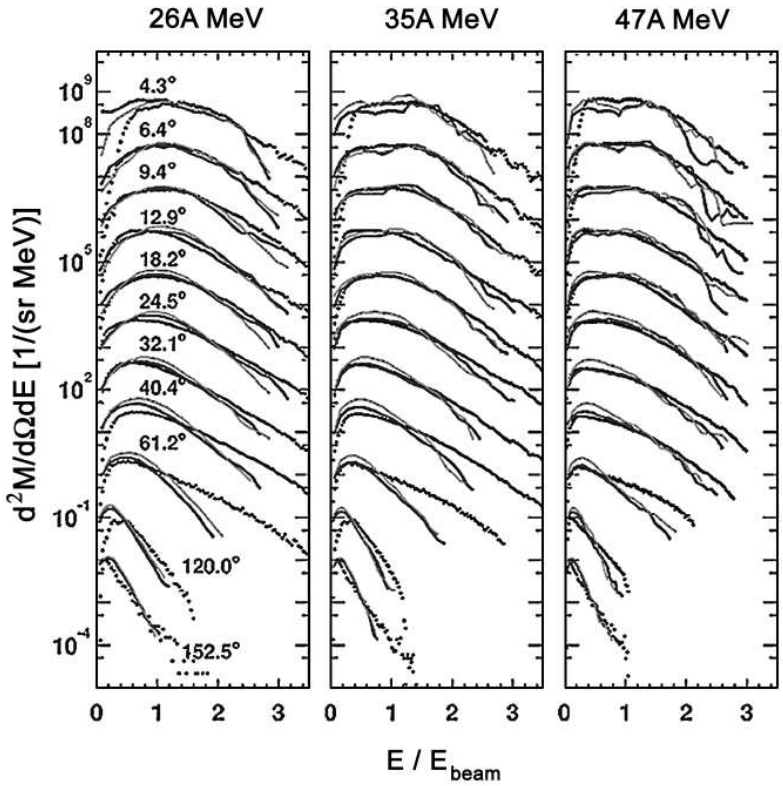

Fig. 12. Proton energy spectra for violent collisions in $^{64}Zr + ^{92}Mo$ reactions at different incident energies (indicated on top) and different detection polar angles (indicated in the left column) are reported. Experimental data are shown by dots. Thick and thin solid lines refer to AMD-V simulation results for soft and stiff EOS with different prescriptions for the in-medium cross-section [3].

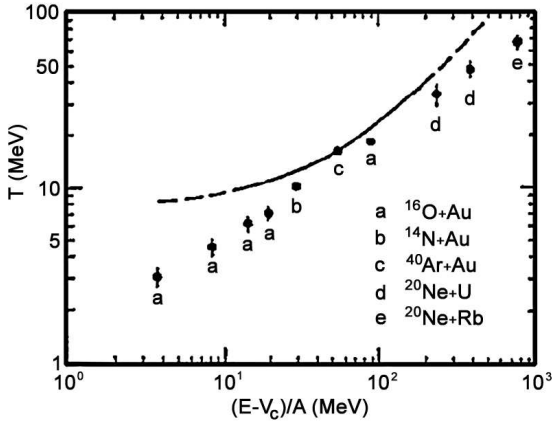

Fig. 13. Experimental slope parameters of the IS in proton spectra for various systems as a function of the bombarding energy above the Coulomb barrier V_c. The curve represents the estimate for quasi-free NN scattering [101].

emission, discussed in the previous paragraph, is found at 10 A·MeV [26].

Originally, the Maxwellian parameterization was introduced following statistical arguments (Boltzmann gas). The momentum distribution components are assumed to be independent Gaussians with a mean square value $\sigma^2 = m \cdot T$, where m is the nucleon mass, and T a temperature parameter. In the case of IS, the parameter T rather represents the random composition of the beam velocity with the Fermi momenta of the nucleons inside the nucleus [101]. The systematics of the extracted slope parameters T for IS for proton spectra is reported in fig. 13 and explained in this framework. Deviations from this picture, especially at low incident energy, have been explained as due to Pauli-blocking effects [101].

By analyzing the neutron energy spectra we expect to find the same characteristics as for protons (the only difference is the lack of Coulomb repulsion). From the experimental point of view neutron detection, especially at high energies, is quite difficult and poor experimental data with respect to charged particles are available. In the $^{35}Cl + ^{nat}Ta$ reaction at 43 A·MeV [102] neutron spectra have been measured up to 50 MeV from 60° to 150° polar angles as a function of the PLF excitation energies and pre-equilibrium neutrons from the IS source have been evidenced. In this work from the Maxwellian fit a IS velocity lower than half the beam velocity for all the PLF excitation energies has been extracted and reproduced by BNV calculations. This trend has been explained as due to the attractive mean field from the target that the emitted neutrons of moderately high energy still feel. In the scenario where pre-equilibrium neutrons are emitted as a consequence of NN collisions, if the emitted neutron un-

dergoes more than one collision, a velocity lower than the NN velocity is expected. Recently, although neutron spectra were measured only up to 25 MeV in the $^{36}\mathrm{Ar} + {}^{58}\mathrm{Ni}$ reaction at 50 A·MeV from 60° to 150° [103], they were analyzed as a function of the centrality and the IS velocity was extracted. The IS velocity is found closer and closer to the NN center-of-mass velocity with increasing centrality. The analysis of proton spectra, presented in the same work but in the $^{58}\mathrm{Ni} + {}^{58}\mathrm{Ni}$ reaction at 52 A·MeV, does not show the same trend; the IS velocity is near to the NN velocity for all the centrality bins. This trend can be explained if neutrons are emitted both from NN collisions in the interaction zone in the first stage of the reaction (predominant at central collisions) and/or by a delayed emission that occurs after the neck rupture and enhanced near the heaviest partner of the reaction thus explaining the lower IS velocity at peripheral and semi-central collisions for neutrons. This delayed emission near the quasi-target is enhanced for neutrons with respect to protons due to the lack of the Coulomb repulsion. To confirm this interpretation simultaneous measurements of protons and neutrons for the same reactions are necessary [104].

An analysis in terms of Maxwellian source emission applied to light-cluster (d, t, He) energy spectra shows a similar scenario. The emission of the most energetic particles from the IS has been explained with a coalescence model where the emission of light clusters is related to the momentum space densities of nucleons in the collision [88,92,93,105]. The coalescence radius, P_0, is the single free parameter of the model once proton and neutron energy spectra are known. P_0 is the radius of a sphere in momentum space where coalescence occurs. Recently, the coalescence model has been coupled with dynamical models describing the collision [98,106,107] to explain the energy spectra of complex light particles. The percentage of particles emitted promptly at intermediate velocity (pre-equilibrium particles) decreases with increasing mass of the cluster [98]. In ref. [106] a self-consistent coalescence model analysis has been used to determine the size of the system as a function of time and to follow the evolution of density and temperature during the reaction. Recently, the emission of light cluster ($Z \geq 3$) at mid-velocities has been interpreted as emitted from a neck-like structure, formed dynamically during the reaction, joining the quasi-projectile and the quasi-target [108,109]. The interest in these studies is focused on understanding the nature of "neck" formation (see the contribution by Di Toro *et al.*, *Neck dynamics*, this topical issue). One of the most relevant features of IMF emission at mid-velocities is a neutron enrichment with respect to IMF emission from the projectile. Four reactions $^{124,136}\mathrm{Xe} + {}^{112,124}\mathrm{Sn}$ [110] were studied at 55 A·MeV supporting the idea that IMFs are emitted from a multiple neck rupture from a material that is "surface-like" thus enhancing the N/Z ratio. These results were confirmed by the chemical analysis of the mid-velocity component measured [100] in peripheral and semi-central collisions induced by Xe and Sn at energies between 25 and 50 A·MeV. The most neutron-rich isotopes are favored at lower energies and in peripheral collisions, where the emission is globally more neutron rich than evaporative processes. Similar results have been found in [111] where more neutron-rich He isotopes are found in mid-peripheral emission from the neck zone with respect to He isotopes emitted from PLF. Exclusive measurements of neutron and proton emission characteristics from intermediate-velocity sources, measured in the same reactions with different N/Z ratio, and comparison with dynamical calculations can add information on the mechanism leading to the neutron enrichment of the neck region.

In the energy regime considered in this review this well-established scenario, in terms of three emitting sources, is a way to mimic the emission of particles dynamically originating during the whole reaction time. In particular, pre-equilibrium particles are not necessarily emitted from a source well located in time. The comparison of experimental data with dynamical model predictions [12] and more complex analyses, as particle-particle correlations (see the contribution by Verde *et al.* in this topical issue and refs. [112,113]) allow to infer a space-time characterization of the emission mechanisms. However, from the experimental point of view, the emitting source parameterization is able to give an estimate of the number of nucleons and of the energy removed at each step in the reaction [95] and to "isolate", by selecting detection angles and energies, energetic particles emitted from the IS (pre-equilibrium particles) for more complex event-based analyses [13,94].

In order to estimate the amount of pre-equilibrium emission, besides the integration of the Maxwellian fitted curves, alternative methods have been applied for the $^{58}\mathrm{Ni}$ on $^{58}\mathrm{Ni}$ reaction at 32 A·MeV [114] in complete events detected with the INDRA apparatus. In this work all the methods applied lead to the same estimate of the mass and the energy removed in the pre-equilibrium stage. In [115] a balance of mass, momentum and energy has been performed for several central reactions with different mass asymmetries and energies (from 17 to 115 A·MeV). These works prove that a large fraction of the initial mass and available energy is removed in the pre-equilibrium stage confirming that the estimate of pre-equilibrium emission is of crucial importance for the study of "hot" systems formed in central heavy-ion collisions. In particular in [116] the isospin content of the pre-equilibrium nucleon emission at high transverse momentum is suggested as a probe to explore the momentum dependence of the symmetry term potential in asymmetric nuclear matter.

The space characterization of pre-equilibrium emission can also be inferred by studying the impact parameter dependence of pre-equilibrium particles [94,117,118]. Energetic protons at large polar angles, measured as a function of the impact parameter for reactions with different mass asymmetry at 44 A·MeV [94], show that pre-equilibrium proton multiplicities increase with the size of the overlapping region and, from system to system, with the number of protons in the collision zone. The trend as a function of impact parameter b can be understood if we assume that proton yields scale with the overlap surface of the colliding system thus indicating that pre-equilibrium protons

are emitted mainly from first NN collisions as already reported for hard-photon emission. This surface dependence had already been predicted for high-energy gamma emission by BUU calculations [31]. In ref. [119] from light particles (p, d, t, ^{3}He and ^{4}He) measured in Ar + Ni collisions from 52 to 95 A·MeV, the amount of matter and energy associated with the IS are estimated. The results indicate that the total mass is directly correlated to the impact parameter and it does not depend on the incident energy, while the energy carried by light particles at intermediate velocity is not strongly dependent on the impact parameter but it depends on the incident energy.

From the analysis of proton angular distributions in reactions with different mass asymmetry at 44 A·MeV [12], a reminiscence of the elementary NN cross-section in the observed anisotropy in central collisions for quasi-symmetric systems confirms the hypothesis that pre-equilibrium protons are emitted as a consequence of first NN collisions. These results, compared with BNV predictions, are consistent with a scenario in which particles are emitted in the first phase of the reaction mainly from the first NN collisions in the interaction zone. Due to the short proton mean free path a strong screening effect is evident, which distorts the expected angular-distribution trends in peripheral reactions and heavy systems. A clear signature of this scenario is provided by γ-p correlation results [54], as described in sect. 2. These results suggest that protons produced in light symmetric systems should be good probes to gather information on the in-medium NN cross-section. Indeed light-cluster formation has been calculated in microscopic transport approaches including nucleon-nucleon cross-section in-medium effects, which depend on the density and energies deposited in the system [120]. This study shows that the number and the spectra of light charged particles change in a significant manner [121,122].

High-efficiency apparatuses are capable of measuring differential energy spectra that span several orders of magnitude. Particles with energy per nucleon up to 3–4 times the incident energy [3,12,13,123] have thus been measured. With the hypothesis that energetic protons are emitted as a consequence of first-chance NN collisions, and that the momentum distribution can be approximated as a degenerate Fermi gas, a kinematical limit in proton energies is expected. The observation in the energy spectra of protons far exceeding this limit is a puzzle not yet resolved. The mechanism able to concentrate in few nucleons so much energy is not yet known, but its knowledge can be of crucial importance to shed light on all sub-threshold particle emission in heavy-ion reaction at intermediate energy. Mechanisms as cooperative effects [15], high-momentum tail of the nucleon Fermi distribution [124], fluctuations in the momentum space [125] or properties of the potential have been proposed. Attempts to reproduce the extremely high-energy tail in proton spectra with dynamical models [3,13,123,125] have been done. In these works, different prescriptions for the effective mean-field potential and for in-medium properties of the two-body collision cross-section have been used.

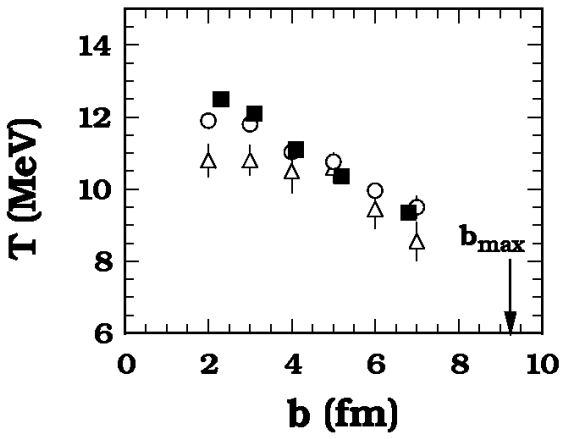

Fig. 14. Inverse-slope parameters extracted from proton spectra as a function of the impact parameter for the ^{58}Ni + ^{58}Ni reaction at 30 A·MeV. Full squares represent the experimental data, open triangles the BNV calculations with a local mean field and open circles the BNV calculations with a momentum-dependent potential [126].

The most promising mechanism responsible for the production of extremely energetic protons seems to be a cooperative mechanism by which more nucleons act together to produce a high-energy nucleon. A similar production of high-energy gamma-rays exceeding the kinematical limit for n-p collisions has been observed in ref. [69]. Experimental inclusive proton spectra measured in Ar + Ta collisions at 95 A·MeV at large polar angles [123] were compared with QMD [125] and BNV [123] calculations that include, besides the usual local mean-field potential and two-body collisions, three-body collisions which succeeded in the explanation of sub-threshold pion production (see section on pions). The comparison with the experimental data shows good agreement in the reproduction of the high-energy slope.

Protons up to twice the NN kinematical limit (5 times the beam energy per nucleon) have been measured as a function of the centrality in the ^{58}Ni + ^{58}Ni reaction at 30 A·MeV. The slope and yield of energetic proton spectra collected at different impact parameters have been extracted and the comparison with results of BNV calculations with a local Skyrme potential and Gale-Bertsh-Das Gupta momentum-dependent potential is reported in fig. 14 [126]. The slopes are well reproduced by a momentum-dependent potential, while the local potential fails especially at central collisions. Since momentum-dependent effects could be expected also from a stiff potential, the dependence on the compressibility term has also been investigated for the same reaction [127]. The proton high-energy spectra predicted by BNV calculations with a hard and a stiff compressibility for a local Skyrme interaction have been compared to the experimental spectra, and the results indicate that the proton spectra are not sensitive to the compressibility term while they are sensitive, both in yield and slope, to a momentum-dependent potential.

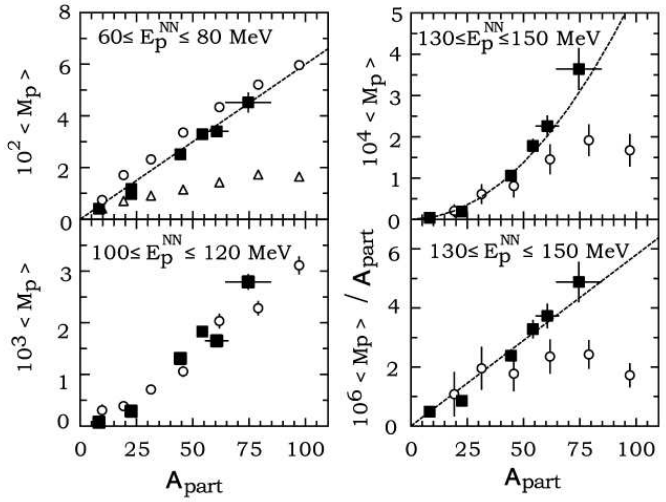

Fig. 15. Proton multiplicities as a function of the number of the participant nucleons (A_{part}) for different proton energies in the reaction ^{58}Ni + ^{58}Ni at 30 A·MeV. Full squares represent the experimental data, open triangles the BNV calculations with a local potential and open circles the BNV calculations with a momentum-dependent potential. In the bottom right panel the points for $130 \leq E_p \leq 150$ are reported, divided by A_{part}. The BNV calculations are scaled by a factor 0.6 in order to take into account the yield reduction due to complex particle emission not predicted by the calculations.

A more detailed analysis for the same reaction has been performed in [13]. High-energy protons were detected in coincidence with heavy fragments in order to select classes of events with different centralities. For each class of events high-energy gamma-rays were measured in coincidence and a quantitative measure of the size of the interaction zone (A_{part}) was determined. In fig. 15 high-energy proton multiplicities as a function of A_{part} (*i.e.* impact parameter) for different energy values are reported. A linear dependence on A_{part} (dashed line in the top left panel) is observed for protons between 60 and 80 MeV, thus confirming that the high-energy proton multiplicity increases linearly with increasing A_{part}. With increasing proton energy a stronger deviation from linearity is observed. The dashed line in the top right panel of fig. 15 shows a quadratic dependence. A similar behavior is observed for π^0 and η at much higher incident energies [128] and interpreted as due to multi-step processes. The experimental data were compared with microscopic BNV calculations where two different potentials were included: a local Skyrme interaction (open triangles in fig. 15) and a Gale-Bertsch-Das Gupta momentum-dependent interaction (open circles). Momentum-dependent BNV calculations reproduce well the data up to 120 MeV (left panels in fig. 15) but fail in reproducing the extremely high-energy proton multiplicity. BNV with local potential undershoot the data already at low energies and central collisions. These results call for the introduction in the transport models of ingredients that are beyond the one- and two-body effects as cooperative effects (three- or higher-order collisions) [15]. As quoted in the introduction, the fact that three-body effects might be important has been advocated also in microscopic Bruckner HF calculations [8] to reproduce the experimental ground-state energy and density of nuclear matter. The information that can be extracted from energetic proton data is that, even though cooperative effects are important, their relevance compared to nucleons produced from two-body collisions is negligible. In BHF microscopic calculations instead the relevance of the three-body force is large, in fact the ground-state density in the calculations decreases almost of a factor two when three-body forces are included [8,129]. We would expect that when increasing the excitation energy of the system three-body forces would become even more important as compared to cold nuclear matter because of some relaxation of the Pauli blocking.

This aspect calls for a further and more detailed experimental and theoretical analysis of these reactions at various beam energies to try to pin down the relevance of two-body *versus* three-body forces, which could be relevant for microscopic calculations of the nuclear-matter EOS and the binding energies of light nuclei.

A detailed comparison between experimental results from several reaction at different incident energies (^{64}Zn + ^{58}Ni, ^{92}Mo and ^{197}Au at 26, 35, 47 A·MeV) with dynamical model predictions has been presented in ref. [3]. The general aim of this work is to get information on the reaction mechanisms by comparing the model results with a wide set of experimental data. Direct experimental observables as velocity and energy spectra, multiplicity and charge distribution for light particles (p, d, t, α) and IMF ($Z \geq 3$) have been compared with a modified antisymmetrized molecular dynamics (AMD-V) that takes into account different prescriptions for the in-medium NN cross-section and a Gogny effective interaction with a momentum-dependent mean field and two different compressibility values. In fig. 12 the experimental proton energy spectra (dots) and AMD-V calculations with two different compressibility values and in-medium NN cross-section description are reported. Results corresponding to a compressibility for infinite nuclear matter $K = 228$ MeV and an empirical in-medium NN cross-section prescription, where no distinction is made between n-n and n-p cross-sections (soft EOS+NN_{emp}) are represented as thick lines while results corresponding to $K = 360$ MeV and an in-medium NN cross section with different-cross section prescription for n-n and n-p cross-sections (stiff EOS+NNLM) are represented as thin lines. Both calculations with different compressibilities are in qualitative agreement with the bulk of data, but none of them is able to reproduce the high-proton energy tails (see fig. 12) especially at around 50° polar angle, which corresponds to emission near 90° in the center-of-mass system, where the high-energy IS component can be clearly evidenced.

5 Conclusions and future perspectives

In this work we have reviewed the production of hard photons, subthreshold pions and energetic nucleons in nucleus-nucleus collisions at intermediate energies

(10 A·MeV $\leq E \leq$ 100 A·MeV). A first remark concerns the fact that the bulk of data are qualitatively rather well reproduced by dynamical calculations like BUU. The nuclear dynamics is described in terms of a mean field and two-body collisions, thus confirming the dominant role of NN collisions, boosted by Fermi motion of the colliding nuclei. This result opened the possibility of carrying on a more detailed comparison between experimental data and calculations in order to put constraints on the in-medium NN cross-section, as well as on the momentum dependence of the nuclear mean field, and on the equation of state of nuclear matter.

As a second general result, the general agreement between high-energy particle data and dynamical transport models calculations qualifies these particles as probes for the early non-equilibrated stage of the reaction. This allows to extract information regarding the pre-equilibrium phase and the following evolution towards equilibration. Some interesting results from a detailed comparison between data and calculations have been obtained:

- a clear evidence of momentum-dependent interactions has been gathered;
- particle production is very sensitive to the NN cross-section, however more work should be done to draw conclusive results on σ_{NN} modifications in the nuclear medium taking also into account the effects on the reaction dynamics.

A word of caution is however necessary. All these conclusions crucially rely on the comparison of data with transport calculations, and one should make clear that they do not depend on the numerical implementation of the model. One main suggestion could be to compare the results of several dynamical calculations with many different experimental data, for example for both energetic nucleon, pion and hard-photon production and, on the other hand, to verify that the same prescriptions allow also a good description of other features of the nucleus-nucleus dynamics both in peripheral (neck, PLF fragmentation, etc.) and central collisions (fusion, multifragmentation, etc.). This procedure should allow to constrain the parameters of interest for the EOS. Moreover, the fact that a probe is sensitive only to some parameters of the EOS and not to others is important since it allows to disentangle the contribution of various parameters. This is the case of hard photons and energetic nucleon spectra that are not particularly sensitive to the stiffness of the EOS.

It is also important to mention that, for energetic proton production, a strong improvement in the agreement between data and calculations is achieved, for central collisions, only including a momentum dependence of the nuclear mean-field interaction. To our knowledge, momentum-dependent calculations have not been carried out for the hard-photon production and, since the effect of Pauli in the final state is much stronger in this case, this comparison is expected to provide additional valuable information.

Hard photons, which are unperturbed probes due to the fact that they once produced do not interact anymore with the surrounding nuclear matter, provide a clean chronology of the various stages of the reaction. In particular, energetic hard photons ($E_\gamma \geq 50$ MeV) gave access to the momentum Fermi distributions of the colliding nuclei in the early non-equilibrated stages of the reaction, while "thermal" hard photons provide a clock for multifragmentation.

The observation of deep-subthreshold or extremely energetic "particles" addressed the question of which mechanisms could allow to concentrate a relevant fraction of the available energy in the production of a single energetic or massive "particle". For hard photons, pions and energetic protons as described in this report, as far as we know, there is a lack of theoretical models to compare with existing deep-subthreshold data. Cooperative effects, where more nucleons or cluster of nucleons participate in the collisions, seem very promising and more theoretical effort should be devoted to this issue. One extreme case which we would like to stress is pionic fusion where all the beam energy is transformed into the pion mass and a compound nucleus is formed very close to its ground state [130].

In the near future the investigation of the isospin degree of freedom will be boosted by the new facilities providing exotic beams and its impact on the EOS of asymmetric nuclear matter will be the next challenge for heavy-ion nuclear physics. In this field, n, p, pion and hard-photon detection is expected to provide very important pieces of information, especially due to the fact that these probes are sensitive to the first stage of the reaction where the largest asymmetry in isospin and densities can be reached. In asymmetric matter a splitting of neutron and proton effective masses is expected, but the sign of the splitting is quite controversial giving opposite results for various Skyrme forces. The investigation of pre-equilibrium particles, for which the high-momentum components have a crucial role, could provide sensitive probes. In particular, the neutron proton ratio of fast nucleon emission as a function of centrality and the slopes and yields of hard-photon spectra, which can provide complementary pieces of information with respect to the nucleon emission thanks to the fact that they are not affected by final-state interaction, should be carried out [131].

Concerning pion emission, several theoretical works have been published, investigating the sensitivity of the π^+/π^- ratio to the isospin degree of freedom at incident energies of about 400 A·MeV, and its dependence on the neutron and proton chemical potentials and on the symmetry energy has been put in evidence [132,133]. However, it is important to underline that these works deal with equilibrated dense nuclear matter, while the possibility of investigating the π^+/π^- ratio at incident nucleon energy below the NN pion energy threshold, could give access to the early non-equilibrated stage of the reaction.

References

1. E. Migneco *et al.*, Nucl. Instrum. Methods. Phys. Res. A **314**, 31 (1992).
2. J. Pouthas *et al.*, Nucl. Instrum. Methods. Phys. Res. A **357**, 418 (1995).

3. R. Wada *et al.*, Phys. Rev. C **69**, 044610 (2004).
4. A. Pagano *et al.*, Nucl. Phys. A **681**, 331 (2001).
5. G. Martinez *et al.*, Nucl. Instrum. Methods. Phys. Res. A **391**, 435 (1997).
6. R.T. De Souza *et al.*, Nucl. Instrum. Methods. Phys. Res. A **295**, 109 (1990).
7. I. Iori *et al.*, Nucl. Instrum. Methods. Phys. Res. A **325**, 458 (1993).
8. W. Zuo *et al.*, Eur. Phys. J. A **14**, 469 (2002); Zuo W. *et al.*, Nucl. Phys. A **706**, 418 (2002).
9. A. Kievski, *Proceedings of the 10th Conference on Problems in Theoretical Nuclear Physics, Cortona 6-9 October 2004* (World Scientific, 2005).
10. A. Bonasera, M. Bruno, C.O. Dorso, P.F. Mastinu, Riv. Nuovo Cimento **23**, 1 (2000).
11. B. Povh, K. Rith, C. Scholz, F. Zetsche, *Particles and Nuclei ? An Introduction to the Physical Concepts* (Springer, 1995).
12. R. Coniglione *et al.*, Phys. Lett. B **471**, 339 (2000).
13. P. Sapienza *et al.*, Phys. Rev. Lett. **87**, 072701 (2001).
14. W. Cassing *et al.*, Phys. Rep. **188**, 363 (1990).
15. A. Bonasera, F. Gulminelli, J. Molitoris, Phys. Rep. **243**, 1 (1994).
16. G.F. Bertsch, S. Das Gupta, Phys. Rep. **160**, 189 (1988).
17. J. Aichelin, Phys. Rep. **202**, 233 (1991).
18. J. Aichelin *et al.*, *Comparison between the different transport codes*, in preparation.
19. J. Julien *et al.*, Phys. Lett. B **264**, 269 (1991).
20. P. Piattelli *et al.*, Nucl. Phys. A **649**, 181c (1996).
21. K.A. Snover, Annu. Rev. Nucl. Part. Sci. **36**, 545 (1986).
22. J.J. Gardhøje, Annu. Rev. Nucl. Part. Sci. **42**, 483 (1992).
23. J.H. Le Faou *et al.*, Phys. Rev. Lett. **72**, 3321 (1994).
24. H. Noll *et al.*, Phys. Rev. Lett. **52**, 1284 (1984).
25. E. Grosse, Nucl. Phys. A **447**, 611c (1985); E. Grosse *et al.*, Europhys. Lett. **2**, 9 (1986).
26. N. Gan *et al.*, Phys. Rev. C **49**, 298 (1994).
27. J. Clayton *et al.*, Phys. Rev. C **40**, 1207 (1989).
28. D. Vasak *et al.*, Nucl. Phys. A **428** (1984).
29. Che Ming Ko, G. Bertsch, J. Aichelin, Phys. Rev. C **31**, R2324 (1985).
30. K. Nakayama, G.F. Bertsch, Phys. Rev. C **36**, 1848 (1987).
31. W. Bauer *et al.*, Phys. Rev. C **34**, 2127 (1986); T.S. Biro *et al.*, Nucl. Phys. A **475**, 579 (1987).
32. B.A. Remington, M. Blann, G.F. Bertsch, Phys. Rev. Lett. **57**, 2909 (1986); B.A. Remington, M. Blann, Phys. Rev. C **36**, 1387 (1987).
33. J.D. Jackson, *Classical Electrodynamics* (J. Wiley and Sons).
34. W. Cassing *et al.*, Phys. Lett. B **181**, 217 (1986).
35. K. Nakayama, Phys. Rev. C **42**, 1009 (1989).
36. H. Huisman *et al.*, Phys. Rev. Lett. **83**, 4017 (1999).
37. M. Volkerts *et al.*, Phys. Rev. Lett. **90**, 062301-1 (2003).
38. M. Volkerts *et al.*, Phys. Rev. Lett. **92**, 202301-1 (2004).
39. N. Herrmann *et al.*, Phys. Rev. Lett. **60**, 1630 (1988).
40. H. Nifenecker, J.P. Bondorf, Nucl. Phys. A **442**, 478 (1985); H. Nifenecker, J.A. Pinston, Annu. Rev. Nucl. Part. Sci. **40**, 113 (1990).
41. R. Shyam, J. Knoll, Nucl. Phys. A **448**, 322 (1986).
42. J. Stevenson *et al.*, Phys. Rev. Lett. **57**, 555 (1986).
43. G. Breitbach *et al.*, Phys. Rev. C **40**, 2893 (1989).
44. C.L. Tam *et al.*, Phys. Rev. C **38**, 2526 (1988).
45. N. Alamanos *et al.*, Phys. Lett. B **173**, 392 (1986).
46. M. Kwato Njock *et al.*, Nucl. Phys. A **489**, 368 (1988).
47. R. Hingmann *et al.*, Phys. Rev. Lett. **58**, 759 (1987).
48. T. Reposeur *et al.*, Phys. Lett. B **276**, 418 (1992).
49. V. Metag, Nucl. Phys. A **488**, 483c (1988).
50. S. Riess *et al.*, Phys. Rev. Lett. **69**, 1504 (1992).
51. E. Migneco *et al.*, Phys. Lett. B **298**, 46 (1993).
52. G. Martinez *et al.*, Phys. Lett. B **334**, 23 (1994).
53. A.R. Lampis *et al.*, Phys. Rev. C **38**, 1961 (1988).
54. P. Sapienza *et al.*, Phys. Rev. Lett. **73**, 1769 (1994).
55. A. Badalá *et al.*, Phys. Rev. Lett. **74**, 4779 (1995).
56. H.W. Barz *et al.*, Phys. Rev. C **53**, R553 (1996).
57. J.H.G. Van Pol *et al.*, Phys. Rev. Lett. **76**, 1425 (1996).
58. P. Piattelli *et al.*, Phys. Lett. B **442**, 48 (1998).
59. V.E. Viola *et al.*, Phys. Rev. C **26**, 178 (1982).
60. A. Schubert *et al.*, Phys. Rev. Lett. **72**, 1608 (1994).
61. F.M. Marqués *et al.*, Phys. Lett. B **349**, 30 (1995).
62. G. Martinez *et al.*, Phys. Lett. B **349**, 23 (1995).
63. D.G. D'Enterria *et al.*, Phys. Rev. Lett. **87**, 022701 (2001).
64. R. Alba *et al.*, Nucl. Phys. A **654**, 761c (1999).
65. R. Alba *et al.*, Nucl. Phys. A **681**, 339c (2001).
66. R. Alba *et al.*, Nucl. Phys. A **749**, 98c (2005).
67. R. Alba *et al.*, arXiv:nucl-ex/0507028, 22-July-2005.
68. D.G. D'Enterria *et al.*, Phys. Lett. B **538**, 27 (2002).
69. K.K. Gudima *et al.*, Phys. Rev. Lett. **76**, 2412 (1996).
70. J. Aichelin, G. Bertsch, Phys. Lett. B **138**, 350 (1984).
71. R. Shyam, J. Knoll, Nucl. Phys. A **426**, 606 (1984).
72. A. Bonasera, G.F. Bertsch, Phys. Lett. B **195**, 521 (1987).
73. W. Bauer, Phys. Rev. C **40**, 715 (1989).
74. A. Badalá *et al.*, Phys. Rev. C **48**, 2350 (1993).
75. W. Benenson *et al.*, Phys. Rev. Lett. **43**, 683 (1979).
76. G.R. Young *et al.*, Phys. Rev. C **33**, 742 (1986).
77. H. Feldmeier, J. Schnack, Rev. Mod. Phys. **72**, 655 (2000).
78. A. Ono *et al.*, Phys. Rev. Lett. **68**, 2898 (1992).
79. M. Papa, T. Maruyama, A. Bonasera, Phys. Rev. C **64**, 024612 (2001).
80. D. Lacroix D. Ph., Chomaz, Nucl. Phys. A **636**, 85 (1998).
81. A. Bonasera, arXiv:nucl-th/0110068.
82. T. Kodama *et al.*, Phys. Rev. C **29**, 2146 (1984).
83. A. Bonasera, F. Gulminelli, Phys. Lett. B **275**, 24 (1992).
84. P. Danielewicz, Q. Pan, Phys. Rev. C **46**, 2002 (1992).
85. J. Aichelin, C.M. Ko, Phys. Rev. Lett. **55**, 2661 (1985)
86. A. Badalá *et al.*, Phys. Rev. C **54**, 2138 (1996).
87. A. Badalá *et al.*, Phys. Rev. C **57**, 166 (1998).
88. T.C. Awes *et al.*, Phys. Lett. B **103**, 417 (1981); T.C. Awes *et al.*, Phys. Rev. C **24**, 89 (1981).
89. T.C. Awes *et al.*, Phys. Rev. C **25**, 2361 (1982).
90. G.D. Westfall *et al.*, Phys. Lett. B **116**, 118 (1982).
91. G.D. Westfall *et al.*, Phys. Rev. C **29**, 861 (1984).
92. B.V. Jacak *et al.*, Phys. Rev. C **35**, 1751 (1987).
93. T. Fukuda *et al.*, Nucl. Phys. A **425**, 548 (1984).
94. R. Alba *et al.*, Phys. Lett. B **322**, 38 (1994).
95. D. Santonocito *et al.*, Phys. Rev. C **66**, 044619 (2002).
96. R. Wada *et al.*, Phys. Rev. C **39**, 497 (1989).
97. B.E. Hasselquist, Phys. Rev. C **32**, 145 (1985).
98. P. Pawlowski *et al.*, Eur. Phys. J. A **9**, 371 (2000) and references therein.
99. J.B. Natowitz *et al.*, Phys. Rev. C **65**, 034618 (2002).
100. E. Plagnol *et al.*, Phys. Rev. C **39** (2000).
101. H. Fuchs, K. Möhring, Rep. Prog. Phys. **57**, 231 (1994).
102. Y. Larochelle *et al.*, Phys. Rev. C **59**, R565 (1999).
103. D. Thieriault *et al.*, Phys. Rev. C **71**, 014610 (2005).

104. R. Ghetti *et al.*, Nucl. Phys. A **674**, 277 (2000).
105. B.V. Jacak *et al.*, Phys. Rev. C **31**, 704 (1985).
106. K. Hagel *et al.*, Phys. Rev. C **62**, 034607 (2000).
107. V. Avdeichikov *et al.*, Nucl. Phys. A **736**, 22 (2004).
108. P.M. Milazzo *et al.*, Nucl. Phys. A **756**, 39 (2005).
109. E. De Filippo *et al.*, Phys. Rev. C **71**, 044602 (2005) and reference therein.
110. J.F. Dempsey *et al.*, Phys. Rev. C **54**, 1710 (1996).
111. P.M. Milazzo *et al.*, Phys. Lett. B **509**, 204 (2001).
112. R. Ghetti *et al.*, Phys. Rev. Lett. **87**, 102701 (2001).
113. G. Verde *et al.*, Phys. Rev. C **65**, 054609 (2002).
114. P. Lautesse *et al.*, Phys. Rev. C **71**, 034602 (2005).
115. Rulin Sun *et al.*, Phys. Rev. Lett. **84**, 43 (2000).
116. J. Rizzo *et al.*, Phys. Rev. C **72**, 064609 (2005).
117. J. Peter *et al.*, Phys. Lett. B **237**, 187 (1990).
118. D. Prindle *et al.*, Phys. Rev. C **48**, 291 (1993).
119. T. Lefort *et al.*, Nucl. Phys. A **662**, 397 (2000).
120. C. Kuhrts *et al.*, Phys. Rev. C **63**, 034605 (2001).
121. E.A. Remler, Ann. Phys. **119**, 326 (1979).
122. E.A. Remler, Phys. Rev. C **25**, 2974 (1982).
123. M. Germain *et al.*, Nucl. Phys. A **620**, 81 (1997).
124. I. Bobeldijk *et al.*, Phys. Lett. B **353**, 32 (1995).
125. M. Germain *et al.*, Phys. Lett. B **437**, 19 (1998).
126. P. Sapienza *et al.*, Nucl. Phys. A **734**, 601 (2004).
127. P. Sapienza *et al.*, LNS Activity Report 2001, p. 46 `www.lns.infn.it`.
128. A.R. Wolf *et al.*, Phys. Rev. Lett. **80**, 5281 (1998).
129. A. Bonasera, *Proceedings of the 10th Conference on Problems in Theoretical Nuclear Physics, Cortona 6-9 October 2004* (World Scientific, 2005) p. 171.
130. D. Horn *et al.*, Phys. Rev. Lett. **77**, 2408 (1996).
131. The Physics Objectives SPIRAL 2 Project (2005) see `www.ganil.fr`.
132. Bao An Li, Phys. Rev. C **67**, 017601 (2003).
133. T. Gaitanos *et al.*, Phys. Lett. B **595**, 209 (2004); G. Ferrini *et al.*, nucl-th/0504032.